Ocean Systems Engineering, *Vol. 15, No. 4 (2025) 407-421*
https://doi.org/10.12989/ose.2025.15.4.407

Rans-based model for simulating hydrodynamic variations around a rigid ship hull

Jules César Ketchakou*[1,2], Dianorré Tokoue Ngatcha[1], Ekmon Mbangue[1], Achille Pandong[2,3] and Sévérin Nguiya[1]

[1]*Mechanic and Materials Laboratory (LGMM) of National Higher Polytechnic school of Douala, University of Douala, P.O.BOX 2107, Douala, Cameroon*
[2]*Department of Marine and Port Engineering, National Higher Polytechnic school of Douala, University of Douala, P.O.BOX 2107, Douala, Cameroon*
[3]*National Advanced School of Maritime and Ocean Science and Technology of University of Ebolowa, Kribi, Cameroon*

(Received September 12, 2025, Revised November 25, 2025, Accepted December 2, 2025)

Abstract. The hydrodynamic variations around floating structures in the naval ship applications are crucial to study its stability and hull optimization. The choice of the hull shape is capital to reduce the dispenses associated with energy. We address one-way fluid–structure interaction for a rigid (fixed) hull under a fluid dynamics model. Structural dynamics are not solved. The developed model is based on the coupling between Reynolds Averaged Navier-Stokes (RANS) equations and a $k-\varepsilon$ turbulence model. This model extends naturally several models available in the literature including classical RANS models (steady and unsteady) and several RANS based models that neglect the turbulence phenomena (including transport and diffusion). The coupled RANS-based model is implemented numerically using finite element methods. We have chosen a two-dimensional ship hull 2D model to show how modelling can address turbulent flows around fixed structure. The numerical results obtained are encouraging and can allow us to study their optimization for the preliminary phase with a certain precision.

Keywords: finite element methods; RANS-based model; rigid ship hull; tests simulation

1. Introduction

The accurate modelling of turbulent flows around submerged structures remains an intriguing challenge. The modeling of turbulent flows around submerged structures is often presented in the form of nonlinear partial differential equations, which precludes the possibility of analytical resolution. A plethora of mathematical models for the resolution of fluid-structure interaction problems can be found in the literature. These models frequently employ Reynolds-Averaged Navier-Stokes (RANS) equations. Mathematical models of the motion of a turbulent flow around a ship hull section have been developed by Pichot (2007), while Marichal (2003) has studied the same phenomenon occurring around a trawl pocket. Some of these models utilize the Reynolds-Averaged Navier-Stokes (RANS) model Ghadini *et al.* (2017), Yari *et al.* (2015). This

*Corresponding author, Ph.D. candidate, E-mail: jcketchakou85@gmail.com

http://www.techno-press.org/?journal=ose&subpage=7 ISSN: 2093-6702 (Print), 2093-677X (Online)

model is constituted by a set of equations that describe the motion of steady or unsteady flows. In cases where the flow is rapid or accelerated, a turbulence model is frequently required. The classical RANS equations, when combined with turbulence equations, are often inadequate for accurately describing turbulent flows that exhibit strong gradients in kinetic energy.

Numerous numerical methods have been developed and employed to solve these models. For example, we may cite the work of Hou *et al.* (2012), Richter (2017), Thai (2023), Abouzar (2023), Saha and Haldar (2024). The fluid is typically solved using the mixed finite element method proposed by Brezzi and Fortin (1991). The structure, which is frequently a plate or a shell, is approximated by finite elements of shell-type. The numerical coupling between the fluid and the structure necessitates the employment of specific algorithms, as elucidated by Teixeira and Awruch (2005) and Wall *et al*. (2022). The implementation of this algorithm is challenging and has been extensively documented in the literature. The interaction between container ships and freak waves in beam seas has been examined by Jiaqian (2023) to demonstrate the impact of freak waves on ships. Hwang (2021) presented a direct simulation of turbulent flows over a bump in an open channel. This was done to examine the turbulence characteristics near divergent waves emanating from the bump and to investigate the interaction of turbulence with the divergent waves. The boundary element method (BEM) may also be employed to evaluate the performance of floating structures in waves, as demonstrated by Maarten and Wellens (2022). It should be noted that the BEM is based on potential flow and has panels along all boundaries of the fluid domain, not only along all boundaries of the floater, in order to make the extension to second order feasible. In Hao (2022), a full-form optimization method based on full parameter modeling is developed. It has been demonstrated that this optimization method is well-suited to the automation of the hull form design process. The aforementioned numerical methods are not effective when computing the turbulent flow structure around complex submerged structures in realistic environments and on general meshes (locally refined). Subsequently, the convergence criteria for the solutions vary according to the type of mesh employed. The study of turbulence flow around the ship hull can facilitate the optimization of all its main dimensions with precision (Abouzar 2023). The hydrodynamic interaction between two or more ships in calm waters has been the subject of study by Muscat-Fenech (2022). In calm waters, the effects of waves and turbulence are not considered. In realistic environments, these effects are not to be discounted. The ship response to hydrodynamic loading has been the subject of study by Le Sourne (2001) and Rudan (2019). While it is possible to obtain a ship response under certain hydrodynamic conditions, this is not the objective of the present work. A simplified fluid-structure interaction model for the assessment of ship hard grounding has been proposed by Kim *et al*. (2022). The aforementioned models are not well-suited for analysis in turbulent flows, including those with significant kinetic energy gradients due to interactions between kinetic energy gradient.

In this study, a numerical investigation is conducted to examine the turbulence characteristics surrounding a ship's hull section profile with the objective of enhancing their design. It is assumed that these structures remain fixed, and that the deformations of the structure due to water forces are not considered (these are the main assumptions). The account for the deformation of the ship hull can be performed in framework of Ngatcha et al's Generalized Formulations (see the famous works Ngatcha *et al*. (2024, 2025), Ngatcha *et al*. (2022, 2024c, 2025) and Mbangue *et al.* (2024)). The first objective of the study was to examine the behavior of turbulent flow around a ship hull section using a RANS-based model. Ultimately, this work will facilitate the enhancement of submerged design. We are convinced that the findings of this study will be of great help in designing of a range of ship hull shape profiles.

The rest of the paper is presented in the following manner. Section 2 is dedicated to presenting the model. Here basis equations and assumptions used in the model are exposed. Section 3 presents the results of numerical tests conducted to evaluate the efficacy of the proposed model.

2. The Mathematical Modeling

2.1 Basis equations

The fluid problem uses the general model of the (mass and momentum) equations of fluid dynamics formulated in terms of velocity/pressure. The fluid is assumed to be incompressible, non-viscous and turbulent. The state of the fluid is in conditions described by the scalar variable pressure. Such a phenomenon is addressed by the continuity equation and the conservation of momentum equation (see Ngatcha (2024a))

$$\begin{cases} \dfrac{\partial \rho}{\partial t} + \dfrac{\partial \left(\rho u_i\right)}{\partial x_i} = 0, \\ \dfrac{\partial \rho u_i}{\partial t} + \dfrac{\partial \left(\rho u_i u_j\right)}{\partial x_j} + \dfrac{\partial p}{\partial x_i} = S_i, \\ \dfrac{\partial u_i}{\partial x_i} = 0, \end{cases} \tag{1}$$

where t is the time, $x_i,\ i=1,2,3$ are the 3D coordinates of the flow u_i, $i=1,2,3$ are the 3D mixing velocity components, ρ is the mixing density and p is the pressure term. The vector S_i is the source term (including hydrodynamic force source term as showed in section 4 below). In that what follows we will use the following notation:
$\left(x_1,x_2,x_3\right)=\left(x,y,z\right)=\left(\mathbf{x},z\right)=X$ and $\left(u_1,u_2,u_3\right)=\left(u,v,w\right)=\left(\mathbf{u},w\right)=U$.

Here the mixing water/air density depends on volume fraction of air and of water α_k (where the subscripts "$k=f,a$" denote the fluid (f) and the air (a) respectively) with $\sum_k \alpha_k = 1$. When $\alpha = 0$ nonwetting phase (air) is considered, when $\alpha \in]0,1[$ two interface (free surface) is considered, when $\alpha = 1$, wetting phase (water) is considered. Then, we have

$$\rho = \sum_k \alpha_k \rho_k \tag{2}$$

where ρ_k is density of phase k .

In compact form the momentum equation in (1) reads

$$\frac{\partial \rho U}{\partial t} + \nabla.\rho(U \otimes U) + \nabla p = S \tag{3}$$

2.2 Reynolds averaged navier-stokes equations

We decompose the velocity field as follows: $u_i = \overline{u}_i + u_i'$, where $\overline{u}_i$ is the Reynolds averaged velocity and u_i' is its fluctuating part.

$$\begin{cases} \dfrac{\partial\left(\overline{\rho}+\rho'\right)}{\partial t}+\dfrac{\partial\left(\overline{\rho}+\rho'\right)\left(\overline{u}_i+u_i'\right)}{\partial x_i}=0, \\ \dfrac{\partial\left(\overline{\rho}+\rho'\right)\left(\overline{u}_i+u_i'\right)}{\partial t}+\dfrac{\partial\left(\overline{\rho}+\rho'\right)\left(\overline{u}_i+u_i'\right)\left(\overline{u}_j+u_j'\right)}{\partial x_j}+\dfrac{\partial \overline{p}}{\partial x_i}=S_i, \\ \dfrac{\partial\left(\overline{u}_i+u_i'\right)}{\partial x_i}=0. \end{cases}$$

By applying the Reynolds averaged procedure of (1) using the velocity decomposition above we find

$$\begin{cases} \dfrac{\partial \overline{\rho}}{\partial t}+\dfrac{\partial\left(\overline{\rho}\overline{u}_i\right)}{\partial x_i}=0, \\ \dfrac{\partial \overline{\rho}\overline{u}_i}{\partial t}+\dfrac{\partial\left(\overline{\rho}\overline{u}_i\overline{u}_j\right)}{\partial x_j}+\dfrac{\partial}{\partial x_j}\left(\overline{\rho' u_i' u_j'}+\overline{\overline{\rho}u_i' u_j'}\right)+\dfrac{\partial \overline{p}}{\partial x_i}=+S_i, \\ \dfrac{\partial \overline{u}_i}{\partial x_i}=0, \end{cases} \tag{4}$$

where the term $\dfrac{\partial}{\partial x_j}\left(\overline{\rho' u_i' u_j'}\right)$ is reformulated as a diffusion term. All these equations can be reduced to the form

$$\frac{\partial \overline{\rho}\phi}{\partial t}+\nabla.\overline{\rho}(\overline{U}\phi)+\nabla\overline{p}=\nabla.(\Gamma_\phi\nabla\phi-\overline{\overline{\rho}U'\otimes\phi'})+S^\phi \tag{5}$$

Here, ϕ can take the value of any scalar. When this scalar is the velocity, $\overline{U}$ the new momentum equations read

$$\frac{\partial \rho\overline{U}}{\partial t}+\nabla.\rho(\overline{U}\otimes\overline{U})+\nabla p^*=\nabla.(\Gamma_\phi\nabla\overline{U}-\overline{\overline{\rho}U'\otimes U'})+S \tag{6}$$

Where $\overline{\rho U'\otimes U'}$ is the Reynolds stress and where p^* is the dynamic pressure term accounting the turbulence, Γ_ϕ is a diffusion coefficient. The Reynolds stress $\overline{\overline{\rho}U'\otimes U'}$ are the terms due to fluctuation velocities and represent the effect of convective transport due to turbulent velocity fluctuation.

The gradient operator reads $\nabla=\left(\dfrac{\partial}{\partial x},\dfrac{\partial}{\partial y},\dfrac{\partial}{\partial z}\right)^T$ and the divergence operator is

$$\nabla.() = \frac{\partial}{\partial x_1} + \frac{\partial}{\partial x_2} + \frac{\partial}{\partial x_3}$$

2.3 Boussinesq assumptions

The assumption of dynamic turbulent viscosity introduced by Boussinesq in 1877 assumes that the Reynolds tensors $\left(\overline{u_i' u_j'}\right)$ can be related to the mean velocity and turbulent viscosity gradients in a manner analogous to that relates the stress and strain tensors of deformations of a Newtonian fluid. According to Boussinesq assumption, we approximate the fluctuation terms due to turbulence as follows

$$-\overline{\overline{\rho} u_i' u_j'} = \mu_t \left(\frac{\partial u_i}{\partial x_j} + \frac{\partial u_j}{\partial x_i} \right) - \frac{2}{3} \mu_t \frac{\partial u_i}{\partial x_i} \delta_{ij} - \frac{2}{3} \overline{\rho} k \delta_{ij}, \quad k = \frac{1}{2} \overline{\left(u_i' u_j' \right)} \tag{7}$$

where k roller kinetic energy , μ_t is the turbulent viscosity that must be modeled (it is often desired that it be positive). The breaking of a wave creates turbulent energy in the form of rollers, which dissipate around the ship. The roller can be well represented by the term given by (6). This energy is not conserved over time. The evolution of the roller turbulent energy is presented below. The dynamic pressure term is given by

$$p^* = \overline{p} + \frac{2}{3} kI \tag{8}$$

where $\overline{p}$ is the averaged pressure. However, the static pressure is simulated.

We also define the turbulent diffusivity which assumes that the Reynolds fluxes of a scalar ϕ are linearly proportional to the mean gradients of this scalar.

$$-\overline{\rho' U' \phi'} = \Gamma_t \nabla \phi, \tag{9}$$

where Γ_t is the turbulent diffusivity $\Gamma_t = \frac{\mu_t}{Pr_t}$, Pr_t the turbulent Prandtl and μ_t the turbulent viscosity. We model incompressible, turbulent flow with an effective viscosity $\mu_{eff} = \frac{\mu_t}{\sigma_{k,\varepsilon}} + \mu$, where μ is molecular viscosity and μ_t is from the k-ε model and $\sigma_{k,\varepsilon}$ is a coefficient (see below). In the $k - \varepsilon$ model, we calculate μ_t as follows

$$\mu_t = C_\mu \rho \frac{k^2}{\varepsilon} \tag{10}$$

with k and ε respectively the kinetic energy and its rate of dissipation given by Wilcox (2006, 2008)

$$\frac{\partial \rho k}{\partial t} + \nabla.\rho(Uk) = \nabla.\left[\left(\mu + \frac{\mu_t}{\sigma_k} \right) \nabla k \right] + P_k - \rho\varepsilon, \tag{11}$$

and

$$\frac{\partial \rho \varepsilon}{\partial t} + \nabla.\rho(U\varepsilon) = \nabla.[(\mu + \frac{\mu_t}{\sigma_\varepsilon})\nabla\varepsilon] + \frac{\varepsilon}{k}(C_{g_1}P_k - C_{g_2}\rho\varepsilon). \tag{12}$$

The term P_k in Eqs. (10) and (11) is the production of turbulence due to the velocity gradients, given by Wilcox (2006)

$$P_k = \mu_t S^2, \quad S = \sqrt{2S_{ij}S_{ij}}, \quad S_{ij} = \frac{1}{2}\left(\partial_i u_j + \partial_j u_i\right) \tag{13}$$

The classical turbulence model given by (10)-(11) incorporates five closure coefficients, which are determined by replacing indeterminate double and triple correlations with algebraic expressions that involve the properties of the mean flow and turbulence. As the flow is confined, we propose the following values for these coefficients, as suggested by Wilcox (2006)

$$c_{g_1} = 1.44; c_{g_2} = 1.92; c_\mu = 0.09; \sigma_k = 1; \sigma_\varepsilon = 1.3. \tag{14}$$

Wall law

In this work, we use the wall law based on the model of Launder and Spalding (1967). This wall law assumes equilibrium between molecular and turbulent phenomena. The production of kinetic energy is maximal, as is the dissipation due to molecular effects. This law can be expressed as follows:

$$U^* = \frac{1}{\kappa}\ln(Ey^*) \tag{15}$$

where $U^* = \frac{\rho\left(C_\mu\right)^{1/4}\left(k_p\right)^{1/2}}{\tau_p}U_p$, $\tau_p = \mu\left(\frac{\partial U}{\partial y}\right)_{wall}$ and $y^* = \frac{\rho\left(C_\mu\right)^{1/4}\left(k_p\right)^{1/2}}{\mu}y_p$,

where $\kappa = 0.42$ is the Von Karman constant the distance to the wall from the first fluid cellular k_p the turbulent kinetic energy to the first fluid cellular, $E = 9.8$ accounting the rugosity of the wall. The hull of the ship is the main source of vorticity and turbulence creation. In regions very close to it, viscosity reduces fluctuations in the tangential velocity component, while turbulence increases rapidly due to the production of kinetic energy caused by significant velocity gradient averages in the outer part of the near-wall region. Accurate modelling of turbulence in these areas will improve the accuracy of numerical solutions.

The final model reads

$$\begin{cases} \frac{\partial \overline{\rho}}{\partial t} + \nabla.\overline{\rho}\overline{U} = \nabla.(\nu\nabla\overline{\rho}), \\ \frac{\partial \overline{\rho}\overline{U}}{\partial t} + \nabla.\overline{\rho}(\overline{U}\otimes\overline{U}) + \nabla p^* = \nabla.(\Gamma_t\nabla\overline{U} - \overline{\rho U^{'}\otimes U^{'}}) + S, \\ -\overline{\rho U^{'}\otimes U^{'}} = \mu_t\left(\nabla U + (\nabla U)^T\right) - \frac{2}{3}\overline{\rho}kI, \quad \Gamma_t = \frac{\mu_t}{Pr_t}, \quad \mu_t = C_\mu\rho\frac{k^2}{\varepsilon}, \quad p^* = \overline{p} + \frac{2}{3}kI \\ \frac{\partial \rho k}{\partial t} + \nabla.\rho(Uk) = \nabla.\left[\left(\mu + \frac{\mu_t}{\sigma_k}\right)\nabla k\right] + P_k - \rho\varepsilon, \\ \frac{\partial \rho\varepsilon}{\partial t} + \nabla.\rho(U\varepsilon) = \nabla.[(\mu + \frac{\mu_t}{\sigma_\varepsilon})\nabla\varepsilon] + \frac{\varepsilon}{k}(C_{g_1}P_k - C_{g_2}\rho\varepsilon). \end{cases} \tag{16}$$

The system (15) is associated with its boundary (of type Neumann) and initial conditions.

Positive schemes (16) are required in terms of convergence and accuracy of the solution. Here, finite element method is used to achieve it.

3. Numerical tests

This section presents a series of simulations designed to illustrate the behavior of turbulent flows around a ship hull section. For the sake of simplicity, both tests are performed using the finite element method the developed model in a two-dimensional context. In this section, we perform the model, which is a two-dimensional version of the system (21) previously developed. In particular, we demonstrate the impact of varying section profiles on the modification of the flow direction. The shape of the hull introduces uncertainty into the flow field around the forward sections of both structures. It is evident that the formation of a vortex represents a challenging phenomenon from a numerical standpoint. In order to analyse the flow behaviour, it is often necessary to use an important criterion that is directly related to the flow characteristics.

A general triangular mesh is employed. The mesh is locally refined, with coarse meshes at the boundaries of the fluid domain and a very fine grid near the hull section. Both sections have been refined to the fluid domain as a whole in order to accurately capture the gradients of the flow field characteristics and strain rate, which vary significantly. The results on fine meshes are more interesting than those on coarse grids because fine meshes can capture small disturbances generated near the ship hull.

For all the tests, the time of simulation is t=100s and the maximum of iterations is 80. The residual tolerance is the order of 10^{-8}. Here, the fluid is water (free surface movement) and the 3D structure is the ship (see Fig. 1). The ship is reduced to its hull represented by a 2D surface (contour) possessing a hydrodynamic profile (see Fig.1 below). The domain of simulation is discretized with 4400 triangular cells. Near the ship hull, we reduced the mesh-size (of 80%) and increased the number of cells. It was observed that all the results converge even when the size of elements tends to zero.

At the entrance to the 2D domain, the Dirichlet conditions $k = 0.01m^2/s^2, \varepsilon = 0.1m^2/s^3$ $\mathbf{u} = (u_d, 0) = (4m/s, 0)$ are imposed; on the lateral boundaries $\boldsymbol{\Gamma}_l$, the Dirichlet conditions

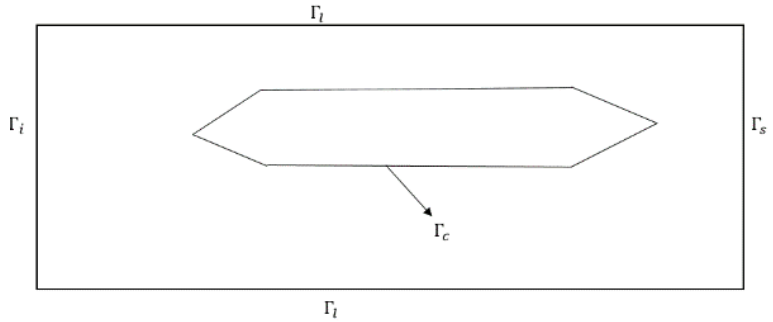

Fig. 1 Geometric of the ship.$\boldsymbol{\Gamma}_l$ is lateral bound, $\boldsymbol{\Gamma}_l$ is the input bound, $\boldsymbol{\Gamma}_s$ is the output bound, $\boldsymbol{\Gamma}_c$ is the Hull of the ship

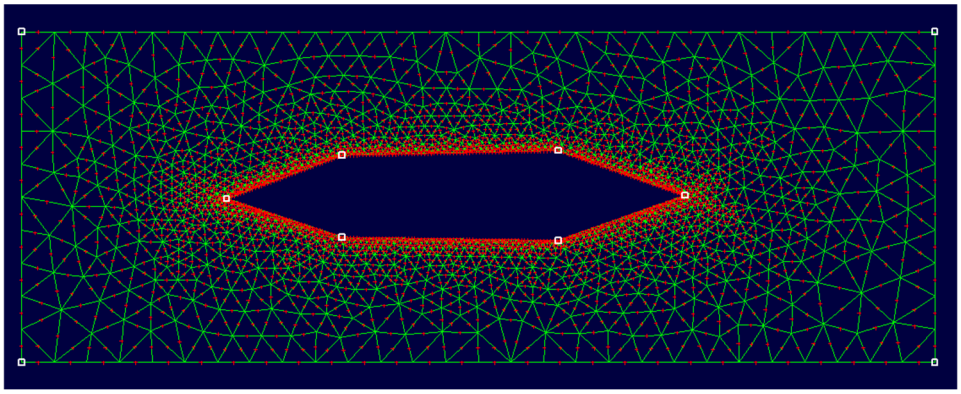

Fig. 2 Locally refined meshes of a ship hull section using 2D Taylor-Hood finite element P_1 / P_2 according to Fig. 1. The ship hull is centered in a fluid domain and the coordinates of the hull are: node 1 (689.245; 405.843), node 2 (689.245; 789.928), node 3, (1752.00; 789.928), node 4 (175,.00; 405,843)

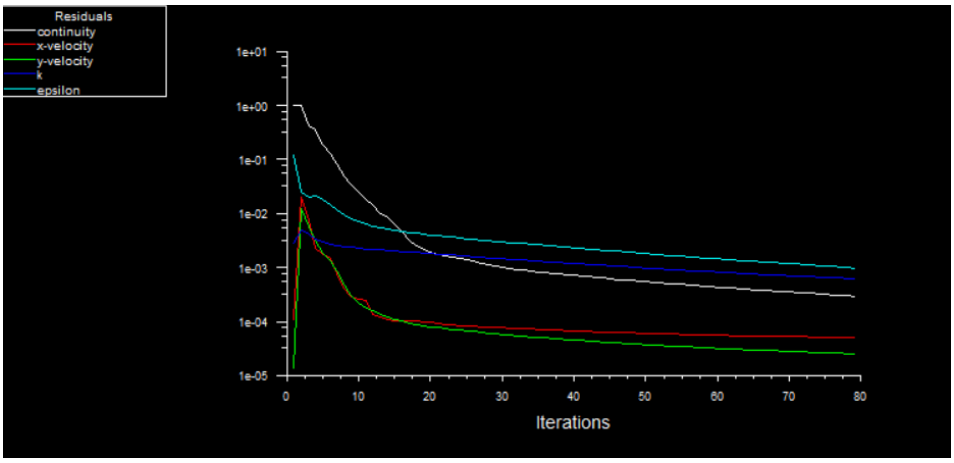

Fig. 3 Computational solution obtained by FEM during 80 iterations. Mass $\overline{\rho}$, horizontal velocities (u and v) and kinetic energy and dissipation

$\bar{\mathbf{u}} = (0,0)$ and $k = 0m^2/s^2, \varepsilon = 0m^2/s^3$ are imposed, and similarly the natural null condition will be imposed at the exit $\boldsymbol{\Gamma}_s$ i.e.

$$\sigma.\mathbf{n} = (p^* I + \nu \frac{(\nabla \bar{\mathbf{u}} + (\nabla \bar{\mathbf{u}})^t)}{2}).\mathbf{n} = 0 \quad \text{at} \quad z = \eta \tag{17}$$

The Eq. (16) is also called dynamic boundary condition at the free surface, where is the Cauchy stress tensor and $\boldsymbol{n}$ the unit normal vector at the free surface.

In regard to the remaining variables, the solution obtained on the subsequent coarser grid was utilized as the initial condition. This approach enables the optimal convergence to be achieved. An

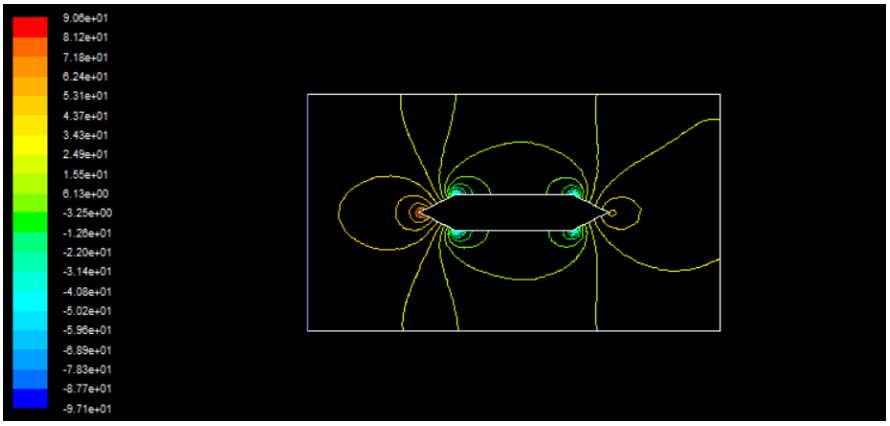

Fig. 4 Contour of Static pressure (Pa). The maximum pressure is $p_{\max} = 90.5Pa$

alternative approach is to utilise a full flow velocity without generating turbulence or acceleration. This methodology has also been employed in the present study. The time step is initially selected to be relatively large and then reduced to a more modest value at the conclusion of the process. During the iterations, the non-linear boundary free surface dynamics equation, as outlined in (16), is applied. The mesh is composed of a Taylor-Hood configuration, which encompasses the ship hull, which is considered the primary obstacle, and the associated force (as source term).

$$F = \int_{\Gamma_{structure}} \sigma.\mathbf{n} ds = \int_{\Gamma_{structure}} \left(p^* I + \left(\frac{\nabla \bar{\mathbf{u}} + (\nabla \bar{\mathbf{u}})^t}{2} \right) \right) ds \tag{18}$$

where the structure is the ship hull or trawl pocket.

We take the flow viscosity as $\nu = 0.003$ and where we apply the condition of adhesion (or condition of non-penetration of water in the ship hull) $\boldsymbol{u}.\boldsymbol{n} = 0$.
During the iterations, the boundary conditions are applied. A convergence has been achieved and the solution for both tests have been calculated and displayed.

The domain of simulation is rectangular and is discretized following Fig. (1).

The results of simulation using finite element methods are plotted in Figs (5)-(10). Here, the turbulent flow behavior of the fluid around the hull ship is showed in our result. A particular attention is paid on the shape of the ship hull.

Fig. (3) illustrates the evolution of the fluid flow characteristic during several iterations to achieve convergence to a stable and steady solution. The flow variables initially exhibit instability in the initial iterations, subsequently attaining stability and constancy after 20 iterations. In these solicited zones, turbulence and velocity exhibit analogous behavior. The velocity declines over time, ultimately reaching zero.

It is observed that all the unknown variables converge to the steady-state solution at a faster rate after a few iterations. It is not necessary to satisfy a convergence criterion for outer iterations, as the solution obtained (a steady-state solution) is not improved.

A detailed examination of Fig. 4 reveals that pressure becomes a significant factor in low-velocity zones, whereas it is relatively insignificant in areas where velocities are highest.

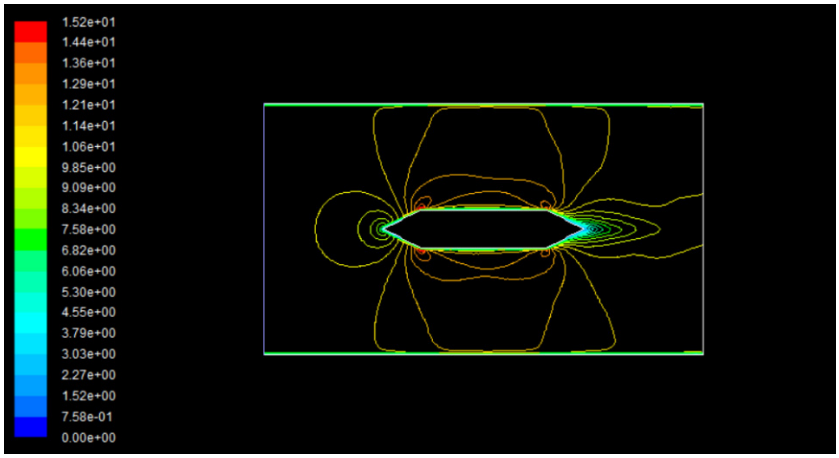

Fig. 5 Contour of the velocity magnitude (m/s)

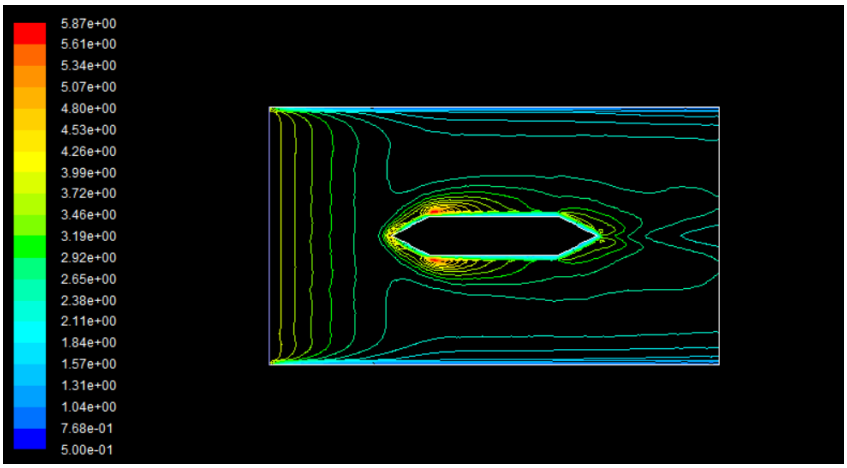

Fig. 6 Contours of Turbulent kinetic energy (TKE). The maximum value of TKE is $k_{max} = 5.82\ m^2/s^2$

This phenomenon can be explained by the underlying fluid mechanics equations. Indeed, when the effects of turbulence are disregarded, the momentum conservation equations yield the following result

$$\nabla \bar{p} = -\frac{\partial \rho \bar{\mathbf{u}}}{\partial t} - \nabla . \rho (\bar{\mathbf{u}} \otimes \bar{\mathbf{u}}) + F \tag{19}$$

From the analysis of Navier-Stokes equations, it can be concluded that pressure gradients increase when advection is of low intensity. This is clearly demonstrated in Fig. 6, which illustrates that the proposed scheme and model are both robust and accurate. At the leading edge of the vessel (Fig. 6), velocity decreases and pressure increases. The pressure gradient exerts a significant influence on the hydrodynamics of the flow, particularly in relation to the shape of the hull.

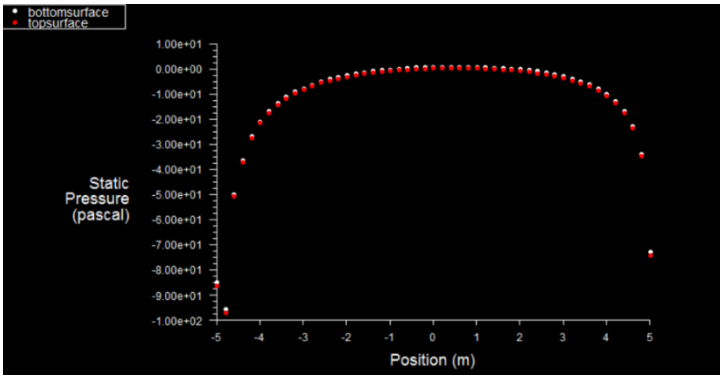

Fig. 7 Static pressure curves

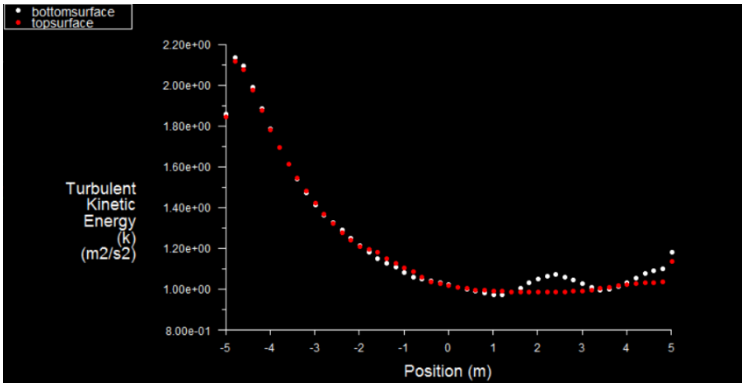

Fig. 8 Turbulence kinetic energy

Fig. (5) shows the variation of the velocity fields around the ship. We can see the zones of high and small velocities of the flow correspond to zone of small and high pressure respectively. Indeed we have from the Eqs. (1) and (18)

$$\frac{\partial \overline{\rho}\overline{\mathbf{u}}}{\partial t} + \nabla.\overline{\rho}(\overline{\mathbf{u}} \otimes \overline{\mathbf{u}}) = -\nabla p^* + \nabla.(\Gamma_t \nabla \overline{\mathbf{u}} - \overline{\rho \mathbf{u}' \otimes \mathbf{u}'}) + F \tag{20}$$

The presence of the ship modifies the wave propagation and in some regions arise strong instabilities and different variations (accelerations and decelerations). Such studies are important to make a preliminaries design to know with which ship profile can reduce considerably the energy dispenses.

Fig. 6 illustrates the behavior of the flow around the ship during the turbulence. It is anticipated that the region of elevated and dispersed turbulence concentrations will be observed. It is notable that the turbulence zones are essentially analogous to those of velocity. This is a logical consequence of turbulence being a function of the square of velocity. This phenomenon is readily discernible in natural settings, as evidenced by the ship's movement through a turbulent flow. Such outcomes, where pronounced kinetic energy gradients are taken into account, are of interest for enhancing the prediction of the ship's propeller resistance.

Fig. 7 illustrates the distribution of the static pressure field in the plane surrounding the structure. It can be observed that the pressure is at its maximum at the entrance. The resistance to the flow of water entering the ship at a velocity is greatest at the front of the vessel, where the flow velocity is lowest. Consequently, the pressure is minimal at this point.

Fig. 8. shows that the kinetic energy is more intense at the position y = - 5 m with a value of order 2.2 m^2 /s^2 decreases to achieve a value of order 1 m^2 / s^2 at the position y = 5 m. We see a slight difference at the position around of y = 2 m and y = 3 m at the bottom and top surface. The results account for the strong interaction between kinetic energy as mentioned above.

General remark

This is clearly demonstrated in the papers referenced in the introduction to this paper. It is reasonable to posit that the shape of the hull may influence the hydrodynamic variables of the fluid (specifically, velocities, kinetic energy, and pressure) and, in turn, affect the stresses associated with ship motion. It would be beneficial to consider the potential for integrating the dynamic behavior of the hull into future investigations. The motion of a ship on water gives rise to turbulence, which is more significant at lower or faster ship speeds. The development of turbulence is contingent upon the shape of the two-dimensional section and the prevailing hydrodynamic conditions.

4. Conclusion

In this paper, we propose a mathematical model of a fluid-structure interaction problem that is capable of describing the motion of turbulent water around a floating structure (including a ship). The model is solved using a finite element method to study the flow behaviour around a 2D hull ship. The study was analysed the flow field characteristic variations around a ship hull section and was investigated the kinetic energy distribution based on the presented system (21). The study will allow the preliminary design of a hull to improve the performance and stability of the vessel during the design project. The model will be used to study the optimisation of the hull profile in order to improve the stability of the ships present in the coastal zones of Cameroon. The proposed fluid-structure equations with fixed structure can be easily extended to more general case studies (ship stability, hull optimisation, etc.) and this is a further investigation. The 3D flow behaviour around a ship with a 3D hull can easily be considered, which is of particular interest for naval applications.

The validation results confirm the reliability of the model, which meets the engineering requirements for simulating the flow field characteristics of a ship hull section. The research demonstrates the complexity of turbulent flow around a hull section.

Future works

The results presented here are only valid when the ship is not deformed by hydrodynamic forces. Future work will include the deformation of the ship as a result of these forces and this

would be a significant addition to the existing work in the literature. Instabilities of the ship in shallow water can also be studied within the framework of Ngatcha (2024a). Shallow water has been shown to affect speed and trim by Carl (1967). The consideration of particles in the water can affect the stability of the ship. A more general model including sediment or other particles can be developed within the framework of Ngatcha *et al.* (2024), Ngatcha (2024b). Finite volume methods can also be used to solve this problem.

Acknowledgments

The authors would like to thank an anonymous referee for giving very helpful comments and suggestions that have greatly improved this paper.

References

Brezzi, F. and Fortin, M. (1991), "Mixed and hybrid finite element methods", **44,** de Springer-verlag, series in computational mathematics springer, berlin, Heidelberg.

Carl, H. (1967), "Effect of shallow water on speed and trim", *Naval Engineers J.*, **79**(2), 271-274.

Cotteleer, L., Longo, R., Debaste, F. and Parente, A. (2024), "Flow-based stress-blended eddy simulation: A local RANS/LES turbulence model for urban flow CFD simulations", *Results in Eng.*, **21**, 101679. https://doi.org/10.1016/j.rineng.2023.101679.

Ebrahimi, A. (2023), "Optimization of a container ship dimensions using multi-objective genetic algorithm method", *Mar. Eng.*, **18**(37), 70-78. https://doi.org/10.52547/marineeng.18.37.70.

Ekmon, M.N., Roland, N.N.A., Renaud, N.G.J., Joseph, N.A. and Robert, N. (2024), "New laminate constitutive equations for analysing the mechanical behavior of anisotropic plates and shells", *Comput. Concrete*, **34**(5), 591-609. https://doi.org/10.12989/cac.2024.34.5.591.

Gabriel, M. and Wellens, P. (2022), "A two-dimensional boundary element method with generating absorbing boundary condition for floating bodies of arbitrary shape in frequency domain", *Int. J. Shipbuild. Progress*, **69**(2), 139-159. https://doi.org/10.3233/ISP-21000.

Gabryuk, V.I. and Kudakaev, V.V. (2020), "Mathematical models that underlie computer simulation of the trawl doors for mid-water trawls", *Ocean Polar Res.*, **42**(1), 77-88. https://doi.org/10.4217/OPR.2020.42.1.077.

Ghadimi, P., Tanha, A., Tavakoli, S. and Feizi Chekab, M.A. (2017), "RANS simulation of the tip vortex flow generated around a NACA 0015 hydrofoil and examination of its hydrodynamic characteristics", *J. Mar. Eng. Technol.*, **17**(2), 106-119. https://doi.org/10.1080/20464177.2017.1330181.

Hao, W., Cong Hong, L., Qiang, L., Xin, Y., Wei, F. and Bi Ye, P. (2022), "Hydrodynamic hull form optimization of a single trawler based on full parametric modeling", *Int. J. Shipbuild. Progress*, **69**(2), 161-179. https://doi.org/10.3233/ISP-22000.

Hou, G., Wang, J. and Layton, A. (2012), "Numerical method for fluid-structure interaction. A review. commun", *Comput. Phys.*, **2**(12), 337-377. https://doi.org/10.4208/cicp.291210.290411s.

Hwang, A., Seok, W. and Lee, S.B. (2021), "Interaction of turbulences with non-breaking divergent waves in an open channel", *Int. J. Naval Arch. Ocean Eng.*, **13**, 35-49. https://doi.org/10.1016/j.ijnaoe.2020.12.004.

Kim, S.J., Sohn, J.M. Kujala, P. and Hirdaris, S. (2022), "A simplified fluid structure interaction model for the assessment of ship hard grounding", *J. Mar. Sci. Technol.*, **27**, 695-711. https://doi.org/10.1007/s00773-021-00862-6.

Launder, B.E. and Spalding, D.B. (1983), "The numerical computation of turbulent flows", *Flow Turbul. Combust.*, **3**(2), 96-116. https://doi.org/10.1016/B978-0-08-030937-8.50016-7.

Le Sourne, H., Donner, R., Besnier, F. and Ferry, M. (2001), "External dynamics of ship-submarine

collision", *Proceedings of international conference on collision and grounding of ships*, Copenhagen, Denmark, 1-3 July 19.
Marichal, D. and Vincent, B. (2008), "Etude dynamique d'un train de pêche complet", *Eur. J. Environ Civil Eng.*, **12**(5), https://doi.org/10.1080/19648189.2008.9693032.
Marichal, D. Etude de l'écoulement dans et au voisinage d'un gonflé par une capture. Etude réalisée pour IFREMER - Contrat 2003-2005.
Muscat-Fenech, C.D., Sant, T., Zheku, V.V., Villa, D. and Martelli, M.A. (2022), "Review of ship-to-ship interactions in calm waters", *J. Mar. Sci. Eng*., **10**(2), 1856. https://doi.org/10.3390/jmse10121856.
Ngatcha, A.R.N. (2024a), "High order shallow water equations: application to dam break problems", *J. Mech*., **40**, 820-842. https://doi.org/10.1093/jom/ufae062.
Ngatcha, A.R.N. (2024b), "A derivation of a 2D PCCU-AENO method for nonconservative problems", *Appl. Eng. Sci*., 100167. https://doi.org/10.1016/j.apples.2023.100167.
Ngatcha, A.R.N. Gnidakouong, J.R.N., Tabejieu, L.M.A. and Feumo, A.G. (2024c), "A 2D exact model by stretching-through-the-thickness a kinematic variable for the 3D exact analysis of laminated composite structures: Theory and applications", *Structures*, **70**, 107445. https://doi.org/10.1016/j.istruc.2024.107445.
Ngatcha, A.R.N., Bandji, D. and Njifenjou, A. (2024d), "Coupling of sediment transport phenomena with turbulent surface flows: Mathematical modeling, finite volume approximation and test-simulations", *Eur. J. Environ. Civil Eng*., **28**(14), 1-34. https://doi.org/10.1080/19648189.2024.2332460.
Ngatcha, A.R.N., Djopkop, L.K., Feumo, A.G. and Nzengwa, R. (2025), "Existence and uniqueness results for well-posed laminated composite shell models", *J. Eng. Math*., **152**(2). https://doi.org/10.1007/s10665-025-10435-w.
Ngatcha, A.R.N., Gnidakouong, J.R.N. and Pandong, A.N. (2022), "A two-dimensional model to analyze the static and dynamic mechanical behavior of multilayered shell structures", *Compos. Struct*., **295**(4), 115754. https://doi.org/10.1016/j.compstruct.2022.115754.
Ngatcha, A.R.N., Ngouanom, G.R., Mbangue, E. and Pandong, A. (2021), "Two dimensional static mechanic analysis of laminated composite tube using ABCDE matriix with no correction factor", *Int. J. Mech*., **1**(15), 107-120. https://doi.org/10.46300/9104.2021.15.12.
Pandong Achille (2023), Lectures notes on stability of ships, National Higher Polytechnic school of Douala, Cameroon,
Park, M.C., Ha, O.K., Ha, S.W. and Jun, Y.K. (2014), "Real-time 3D simulation for the trawl fishing gear based on parallel processing of sonar sensor data", *Int. J. Distrib. Sens. N.*, Article ID 242185,9. https://doi.org/10.1155/2014/24218.
Pichot, G. (2007), "Modélisation de l'écoulement autour d'une poche de chalut", ESAIM: Proceedings, Octobre 22, 132-139.
Priour, D. (2003), "Analysis of nets with hexagonal mesh using triangular elements", *Int. J. Numer. Method. Eng*., **56**(12), 1721-1733. https://doi.org/10.1002/nme.635.
Raviart, P.A. and Thomas, J.M. (1988), Introduction à l'analyse numérique des équations aux dérivées partielles, Edition Masson.
Richter, T. (2017), "Fluid-Structure interactions: Models Analysis and finite element", **118**.
Rudan, S., Catipovic, I., Berg, R., Völkner, S. and Prebeg, P. (2019), "Numerical study on the consequences of different ship collision modelling techniques", *Ships Offshore Struct*., **14**(1), 387-400. https://doi.org/10.1080/17445302.2019.1615703.
Saha, S. and Haldar, B. (2024), "Computational analysis on fluid flow characteristics in a modified annular dump combustor of a ship", *Results in Eng*., **21**, 101723. https://doi.org/10.1016/j.rineng.2023.101723.
Shih, T.H., Liou, W.W., Shabbir, A., Yang, Z. and Zhu, J. (1995), "A new k-ϵ eddy viscosity model for high reynolds number turbulent flows", *Comput. Fluids*, **24**(3), 227-238. https://doi.org/10.1016/0045-7930(94)00032-T.
Shirkavand, A. and Farrahi-Moghaddam, K. (2024), "The application of a non-hydrostatic RANS model for simulating irregular wave breaking on a barred and sloping beach", *Results in Eng*., **23**, 102451. https://doi.org/10.1016/j.rineng.2024.102451.
Song, Y.J. and Woo., J.H. (2013), "New shipyard layout design for the preliminary phase case study for the

green field project", *Int. J. Naval Arch. Ocean Eng*., **5**(1), 132-146.
Sprenger, F., Maron, A., Delefortrie, G., Zwijnsvoorde, T.V., Cura-Hochbaum, A., Lengwinat, A. and Papanikolaou, A. (2017), "Experimental studies on seakeeping and maneuverability of ships in adverse weather conditions", *J. Ship Res*., **61**(3),131-152. https://doi.org/10.5957/JOSR.170002.
Texeira, P.R.F. and Awruch, A.M. (2005), "Numerical simulation of fluid-structure interaction using the finite element method", *Comput. Fluid*, **34**(2), 249-273. https://doi.org/10.1016/j.compfluid.2004.03.006.
Tran, T.G., Nguyen, H.V. and Huynh, Q.V. (2023), "A method for optimization the hull form of fishing vessels", *J. Ship Res*., **67**(1),72-91. https://doi.org/10.5957/JOSR.05210017.
Wall, A., Thornhill, E., Barber, H., McTavish, S. and Lee, R. (2022), "Experimental investigations into the effect of at sea condition on ship airwake characteristics", *J. Wind Eng. Ind. Aerod*., **223**, 104933. https://doi.org/10.1016/j.jweia.2022.104933.
Wang, J., Qin, H., Hu, Z. and Mu, L. (2023), "Three-dimensional study on the interaction between a container ship and frak waves in beam sea", *Int. J. Naval Arch. Ocean Eng*., **15**, 100509.
Wilcox, D.C. (2006), Turbulence modeling for CFD, 3rd Ed., DCW industries La Canada, CA.
Wilcox, D.C. (2008), "Formulation of the k-w turbulence model revisited", *AIAA J*., **46**(11), 2823-2838. https://doi.org/10.2514/1.36541.
Yari, E. and Ghassemi, H. (2015), "The unsteady hydrodynamic characteristics of a partial submerged propeller via a RANS solver", *J. Mar. Eng. Technol*. **14**(3), 111-123. https://doi.org/10.1080/20464177.2015.1117717.

MK